DOI: 10.1534/genetics.105.046144

Capture of Extranuclear DNA at Fission Yeast Double-Strand Breaks

Anabelle Decottignies[1]

Cellular Genetics, Christian de Duve Institute of Cellular Pathology, Catholic University of Louvain, 1200 Brussels, Belgium

Manuscript received June 10, 2005
Accepted for publication August 23, 2005

ABSTRACT

Proper repair of DNA double-strand breaks (DSBs) is necessary for the maintenance of genomic integrity. Here, a new simple assay was used to study extrachromosomal DSB repair in *Schizosaccharomyces pombe*. Strikingly, DSB repair was associated with the capture of fission yeast mitochondrial DNA (mtDNA) at high frequency. Capture of mtDNA fragments required the Lig4p/Pku70p nonhomologous end-joining (NHEJ) machinery and its frequency was highly increased in fission yeast cells grown to stationary phase. The fission yeast Mre11 complex Rad32p/Rad50p/Nbs1p was also required for efficient capture of mtDNA at DSBs, supporting a role for the complex in promoting intermolecular ligation. Competition assays further revealed that microsatellite DNA from higher eukaryotes was preferentially captured at yeast DSBs. Finally, cotransformation experiments indicated that, in NHEJ-deficient cells, capture of extranuclear DNA at DSBs was observed if homologies—as short as 8 bp—were present between DNA substrate and DSB ends. Hence, whether driven by NHEJ, microhomology-mediated end-joining, or homologous recombination, DNA capture associated with DSB repair is a mutagenic process threatening genomic stability.

DNA double-strand breaks (DSBs) are genotoxic lesions, which can be caused either by external agents such as ionizing radiations or radiomimetic drugs or by physiological cellular processes such as V(D)J recombination (Roth *et al.* 1992) or meiosis (Sun *et al.* 1989; Cao *et al.* 1990). Replication fork collapse during DNA replication provides another source of DSBs (Michel *et al.* 1997). Proper repair of chromosome breaks is necessary to prevent genomic rearrangements, a hallmark of cancer cells, or cell death. Cells from all organisms have evolved several mechanisms to reseal DSBs. Homologous recombination (HR) is the main pathway for DSB repair in yeast. It is mainly error free and requires the *RAD52* epistasis group of genes including *Saccharomyces cerevisiae RAD51* and *Schizosaccharomyces pombe rhp51*$^+$, two orthologs of bacterial *RecA* (Pâques and Haber 1999). Mammalian cells are thought to rely preferentially on nonhomologous end-joining (NHEJ) for DSB repair, a mechanism that seals two broken ends in the absence of extended sequence homology. In all organisms, NHEJ requires, among others, the heterodimeric DNA-binding proteins Ku70 and Ku80 (*S. pombe* Pku70p and Pku80p) and DNA ligase IV (*S. pombe* Lig4p). More recently, studies in NHEJ-deficient cells, including yeast (Boulton and Jackson 1996; Manolis *et al.* 2001; Ma *et al.* 2003; Yu and Gabriel 2003), mammalian (Feldmann *et al.* 2000; Zhong *et al.* 2002; Bentley *et al.* 2004; Guirouilh-Barbat *et al.* 2004), or plant cells (Heacock *et al.* 2004), revealed the existence of an alternative *KU70/KU80*- and *RAD52*-independent microhomology-mediated end-joining mechanism (MMEJ). This error-prone mechanism relies on the presence of DNA microhomologies (often imperfect) for ligation, leading to deletions during the complementary search (Feldmann *et al.* 2000; Manolis *et al.* 2001; Ma *et al.* 2003; Yu and Gabriel 2003; Bentley *et al.* 2004). In budding yeast, microhomologies at MMEJ junctions (~11 bp) are longer than the typical overlapping sequences (<5 bp) found at NHEJ junctions but shorter than the ~30 bp thought to be required for *RAD52*-dependent HR (Kramer *et al.* 1994; Manivasakam *et al.* 1995; Boulton and Jackson 1996; Ma *et al.* 2003; Yu and Gabriel 2003). Further evidence for *in vivo* MMEJ repair of DSBs has been provided in Ku-deficient mice where some V(D)J recombination still persists and is associated with extensive deletions at repair junctions (Gu *et al.* 1997). Although genetic and biochemical experiments, including the dissociation of NHEJ from MMEJ activity by fractionation of calf thymus cell extracts (Mason *et al.* 1996), have suggested that the two DNA repair mechanisms rely on distinct enzymes, the genetic requirements for MMEJ remain largely elusive. Two recent studies in *S. cerevisiae* and Arabidopsis (Ma *et al.* 2003; Heacock *et al.* 2004) reported a reduced frequency of MMEJ in the absence of the conserved Mre11 complex (*S. cerevisiae* Mre11p/Rad50p/Xrs2p, human Mre11/Rad50/Nbs1, and *S. pombe* Rad32p/Rad50p/Nbs1p), a complex further involved in DNA damage checkpoint signaling and HR- and NHEJ-mediated DSB repair (D'Amours and Jackson 2002). Whereas loss of the Mre11 complex strongly decreases

[1]*Address for correspondence:* Cellular Genetics, Christian de Duve Institute of Cellular Pathology, Catholic University of Louvain, Ave. Hippocrate 74+3, 1200 Brussels, Belgium.
E-mail: anabelle.decottignies@gece.ucl.ac.be

the efficiency of DSB repair in budding yeast (Schiestl *et al.* 1994; Moore and Haber 1996; Boulton and Jackson 1998; Ma *et al.* 2003), extrachromosomal DSB repair assays have suggested that it has either little or no effect on the frequency of NHEJ-mediated repair of linearized plasmids in fission yeast (Wilson *et al.* 1999; Manolis *et al.* 2001).

From yeast to mammals, studies have reported the insertion of DNA fragments of various sources at experimentally induced DSBs, including mitochondrial DNA (mtDNA) and retrotransposons in yeast (Teng *et al.* 1996; Ricchetti *et al.* 1999; Yu and Gabriel 1999) and repetitive DNA (Sargent *et al.* 1997; Salomon and Puchta 1998; Lin and Waldman 2001a), microsatellite DNA (Liang *et al.* 1998; Lin and Waldman 2001a), or the vector encoding the I-*Sce*I endonuclease used to create the DSB in higher eukaryotic cells (Sargent *et al.* 1997; Liang *et al.* 1998; Salomon and Puchta 1998; Lin and Waldman 2001a,b; Allen *et al.* 2003). Interestingly, recent studies reported the association of human genetic diseases with *de novo* insertions of mtDNA in the nuclear genome (Willett-Brozick *et al.* 2001; Borensztajn *et al.* 2002; Turner *et al.* 2003; Goldin *et al.* 2004). Reported cases included a patient exposed to Chernobyl radiation, suggesting that DSB repair-driven chromosomal integration of mtDNA may not occur exclusively under experimental conditions. Finally, systematic sequencing of nuclear genomes from budding yeast, human, and various plant species revealed that integration of mtDNA fragments occurred during evolution and is probably an ongoing process (Ricchetti *et al.* 1999, 2004; Mourier *et al.* 2001; Woischnik and Moraes 2002; Richly and Leister 2004). It is noteworthy that mtDNA insertion has also been detected in the coding sequence of the *c-myc* oncogene in HeLa cells, providing a potential mechanism for tumorigenesis (Shay and Werbin 1992). Similarly, the capture of microsatellite DNA at mammalian DSBs not only has been reported experimentally (Liang *et al.* 1998; Lin and Waldman 2001a) but also was detected at the breakpoints of lymphoid tumor-specific translocations (Boehm *et al.* 1989). Insertion of microsatellite DNA at DSBs provides a source of genomic instability as DNA repeats are prone to expansions/contractions during cellular processes like DNA replication or DSB-induced gene conversion (Richards and Sutherland 1997; Richard *et al.* 1999).

In this study, I investigated genetic requirements and DNA substrates for DSB repair in *S. pombe* using a new simple extrachromosomal (EC) DSB repair assay. In particular, I wanted to clarify the role of the fission yeast Mre11 complex in DSB repair. The assay revealed the association of EC DSB repair with NHEJ-dependent capture of fission yeast mtDNA, a process also requiring the Mre11 complex. Next, the EC DSB repair assay was used to screen for DNA sequences from higher eukaryotes that may be preferentially captured at DSBs. Finally, I compared the relative efficiencies of NHEJ, MMEJ, and HR for insertion of DNA substrates at DSBs in fission yeast.

MATERIALS AND METHODS

Fission yeast strains and methods: The *S. pombe* strains used in this study are described in Table 1. The KT1a0 and KT120 strains were kindly provided by Masaru Ueno. The PN559, PN2490, and PN3773 strains were provided by Paul Nurse. Cells were cultured at 32° in rich (YE5S) or Edinburgh minimal (EMM2) media and sporulated on malt extract media as described in Moreno *et al.* (1991). Yeast transformations were performed using the lithium acetate method as described in Okazaki *et al.* (1990). Specifically, cells grown to a density of 5–20 $\times$ 10^6 cells/ml in YE5S were harvested, washed twice with 20 ml LiOAc 0.1 M (pH 4.9), and resuspended to a final concentration of 2 $\times$ 10^9 cells/ml in LiOAc 0.1 M. Aliquots of 100 μl were incubated at 25° for 1 hr before addition of DNA and another 1-hr incubation at 25°. Cells were mixed with 290 μl 50% PEG 3350/LiOAc 0.1 M and incubated at 25° for 1 hr. After heat shock at 43° for 15 min, followed by incubation at 25° for 10 min, cells were washed with water and directly plated onto selective medium. Exponentially growing cells refer to overnight yeast cultures grown to a final density of 5–20 $\times$ 10^6 cells/ml YE5S and cells in stationary phase were obtained by incubating exponentially growing cells (5–20 $\times$ 10^6 cells/ml) for another 24 hr at 32° without changing the culture medium at a final density of 50–100 $\times$ 10^6 nondividing cells/ml.

DNA for yeast transformation: The 1747-bp *S. pombe ura4*$^+$ gene was PCR amplified on REP4 plasmid (Maundrell 1993) with 5′-TAGCTACAAATCCCACTGGC and 5′-TTGACGAAACT TTTTGACAT and *Taq* polymerase (Takara, Berkeley, CA). To get the pUC18::*ura4*$^+$ plasmid, the *S. pombe ura4*$^+$ gene was PCR amplified on REP4 plasmid with 5′-TTATAGATCTGTTT TATCTTGTTTGTCTACATGG and 5′-TGCATGGATCCTAAA AAAGTTTGTATAGATTATTT, digested with *Bgl*II and *Bam*HI, and cloned into *Bam*HI-cleaved pUC18 plasmid. I used 1 μg of *Eco*RI-linearized pUC18::*ura4*$^+$ plasmid for yeast transformation. In cotransformation experiments, yeasts were transformed with 2 μg *ura4*$^+$ DNA and 2 μg cotransforming DNA (1:1 weight ratio) obtained as follows: the 600-bp mtDNA fragment (position 4501–5100 on the fission yeast mtDNA map) was PCR amplified on wild-type cells (PN559) with 5′-AACCG TAGTGGAAGTTGCGGTTGAACTAAT and 5′-ATAAGTATAC CATGTGCTGAGATTGCAACA; the 250-bp human genomic DNA fragment flanked by 8 bp of microhomology to *S. pombe ura4*$^+$ 5′ and 3′ extremities was amplified by PCR on clone 7 (described in Figure 5D) with 5′-TTCGTCAACTGTACA and 3′-ATTTGTAGATATAATATATATTTG (microhomologous nucleotides are underlined). To obtain the 856-bp DNA fragment containing long stretches of homology to *ura4*$^+$, the same piece of human genomic DNA was PCR amplified on clone 7 with 5′-CACCATGCCAAAAATTACAC and 5′-TTGG TTGGTTATTGAAAAAGTCG. For cotransformation experiments with salmon or human genomic DNA, cells were transformed with 2 μg *ura4*$^+$ DNA and 50 μg of either sheared salmon sperm DNA (Sigma, St. Louis), or human genomic DNA extracted from 293 human embryonic kidney cells (QIAamp kit, QIAGEN, Chatsworth, CA).

Identification of *ura4*$^+$ circular DNA junctions: Junctions in *ura4*$^+$ circles were PCR amplified on boiled yeast colonies with 5′-TTAGAGAAAGAATGCTGAGTA and 5′-TTGGTTGGTTAT TGAAAAAGTCG, yielding 489-bp-long PCR products for intact junctions. More internal primer (5′-CACCATGCCAAAAATTAC AC) was used to amplify truncated junctions in NHEJ-deficient

TABLE 1

Yeast strains used in this study

Strain	Genotype	Source
PN559	*h⁻ leu1-32 ura4-D18 ade6-M216*	P. Nurse's lab collection
PN2490	*h⁺ ura4-D18 rhp51Δ::kan^R*	P. Nurse's lab collection
PN3773	*h⁺ leu1-32 ura4-D18 his3-D1 ade6-M210 pku70Δ:: kan^R*	Baumann and Cech (2000)
KT1a0	*h⁺ leu1-32 ura4-D18 ade6-M210 lig4Δ::LEU2*	Tomita *et al.* (2003)
KT120	*h⁺ leu1-32 ura4-D18 ade6-M210 rad50Δ::LEU2*	Tomita *et al.* (2003)
AD459	*h⁻ leu1-32 ura4-D18 ade6-M216 lig4Δ::LEU2*	PN559 × KT1a0
AD462	*h⁺ leu1-32 ura4-D18 ade6-M216 lig4Δ::LEU2 pku70Δ:: kan^R*	AD459 × PN3773

cells. PCR products were purified from agarose gel and sequenced using the DYEnamic sequencing kit from Amersham Biosciences.

Observation of mitochondria in living cells: *S. pombe* wild-type cells (PN559) were transformed with plasmid TA25 (kindly provided by Yasushi Hiraoka) containing a fusion between the 5′-end of the *atp3⁺* gene, encoding a subunit of the fission yeast mitochondrial ATP synthase and GFP (Ding *et al.* 2000). Mitochondria fluorescence was observed *in vivo* with a Zeiss Axioplan microscope, using a 100×, 1.3 oil immersion lens. GFP was excited with a mercury lamp, using a HQ 450/50 filter (Chroma, Brattleboro, VT). A HQ 510/50 filter was used for fluorescence emission and images were captured with a Hamamatsu 3CCD chilled camera and processed with Adobe PhotoShop 6.0 software (Adobe Systems, San Jose, CA).

DNA sequence comparison: Sequences of *ura4⁺* circle inserts were compared to NCBI nonreductant database using BLAST software (http://www.ncbi.nlm.nih.gov:80/blast). Fission yeast *nu*clear DNA sequences of *mit*ochondrial origin (NUMTs) were detected through BLAST search against the *S. pombe* nuclear genome (http://www.sanger.ac.uk/cgi-bin/blast/submitblast/s_pombe/) using mtDNA genome (accession no. X54421) as query. The selection criteria were a minimal NUMT size of 22 bp with an identity to mtDNA ≥85%.

RESULTS

Extrachromosomal DSB repair assay: So far, study of EC DSB repair in eukaryotic cells has relied on endonuclease-cleaved plasmid as substrate. Here, I tested whether the extremities of a PCR-amplified piece of DNA may be recognized as DSB and processed by the DNA repair machinery of the cell. One advantage of the system lies in the possibility of adding selected nucleotide sequences to 5′-ends of primers to monitor the repair of various DSB end sequences.

To test the feasibility of the system, exponentially growing *ura4-D18 S. pombe* cells were transformed with 1747-bp PCR-amplified *ura4⁺* DNA composing the *S. pombe ura4⁺* ORF flanked by 528 bp upstream of the ATG and 426 bp downstream of the STOP codon (Figure 1A), a fragment with no homology to the nuclear genome of *ura4-D18* cells. Grimm and Kohli (1988) reported that, although devoid of a known autonomously replicating sequence, the *ura4⁺* DNA replicates autonomously in fission yeast. Transformation of 2×10^8 wild-type cells with 2 μg *ura4⁺* PCR fragment yielded an average of 4800 Ura⁺ colonies. This number was reduced to 0–100 Ura⁺ colonies in *lig4Δ* and *pku70Δ* NHEJ-deficient strains. The instability of most Ura⁺ colonies (~90% after two replica platings onto nonselective medium) suggested that the *ura4⁺* DNA was not integrated at high frequency into the genome. Accordingly, ~70% (221/317) of the wild-type Ura⁺ colonies gave a PCR product after amplification with primers in the 5′ and 3′ regions of *ura4⁺* designed to amplify *ura4⁺* junctions resulting from intramolecular ligation (Figures 1A and 3A). Circularization of *ura4⁺* DNA was confirmed by Southern blot analysis of total DNA isolated from both wild-type and *rad50Δ* Ura⁺ cells (data not shown). Therefore, it appears that the *ura4⁺* fragment ends were indeed recognized as DSB and subjected to end-joining. The absence of PCR product in a subset of Ura⁺ clones may be, at least partially, due to the presence of long extranuclear DNA inserts (see below). To compare *ura4⁺* circularization efficiency in different yeast genetic backgrounds, I calculated the ratio of repair events to transformation efficiency. This was achieved by transforming cells with either 1 μg PCR-amplified *ura4⁺* (1.7 kb) or 1 μg uncut REP4 [*ura4⁺*] plasmid (8.5 kb) (*ura4⁺* PCR/REP4 molar ratio of 5) as control for transformation efficiency (Figure 1B). Circularization efficiency was then calculated as the ratio of Ura⁺ colonies obtained with PCR-amplified *ura4⁺*/Ura⁺ colonies obtained with REP4. In wild-type cells, the ratio was of 96% ± 32%. The *ura4⁺* circularization efficiency was not affected in *rhp51Δ* and *rad50Δ* cells (Figure 1B) even though the number of Ura⁺ colonies obtained after transformation with either *ura4⁺* DNA or REP4 uncut plasmid was reduced compared to wild-type cells. To rule out the possibility that the presence of more than one molecule of *ura4⁺* DNA in the nucleus may mask an intramolecular ligation deficiency of *rad50Δ* cells, wild-type and *rad50Δ* cells were transformed with decreasing amounts of *ura4⁺* and REP4 DNA (down to 0.1 μg). Strikingly, circularization efficiencies were similar in both strains at all DNA concentrations tested (Figure 1C).

In *lig4Δ* and *pku70Δ* cells, however, *ura4⁺* circularization efficiency was reduced to 1.2% and 0.2% of the wild-type value, respectively (Figure 1B), in agreement with the *pku70⁺* and *lig4⁺* requirement for efficient end-joining activity. The *lig4Δpku70Δ* double mutant did not

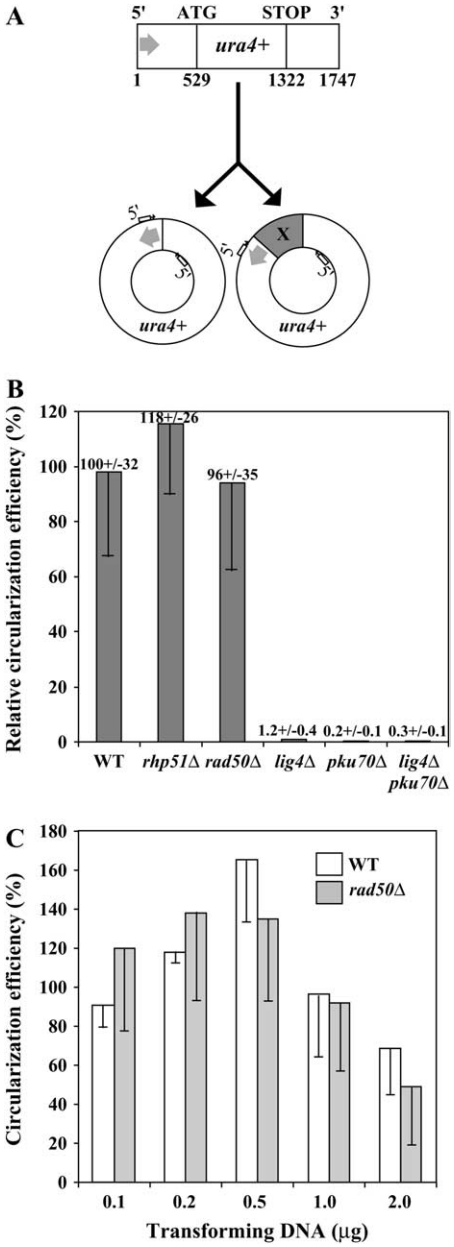

FIGURE 1.—A new extrachromosomal DSB repair assay in *S. pombe*. (A) A 1747-bp PCR-amplified DNA fragment containing the *S. pombe ura4*$^+$ gene was used as substrate to monitor EC DSB repair in fission yeast. Circularization of *ura4*$^+$ DNA occurred with or without insertion of DNA fragments (X). (B) The number of yeast Ura$^+$ colonies obtained after transformation of wild-type (PN559), *rhp51*Δ (PN2490), *rad50*Δ (KT120), *lig4*Δ (AD459), *pku70*Δ (PN3773), and *lig4*Δ*pku70*Δ (AD462) cells with 1 μg of either *ura4*$^+$ PCR product or REP4[*ura4*$^+$] uncut plasmid was monitored in at least four independent transformations. Circularization efficiencies were calculated as the ratio of Ura$^+$ colonies obtained with both transforming DNA species (*ura4*$^+$ PCR product/REP4). Values were compared to the wild-type efficiency (WT = 100%). (C) *Ura4*$^+$ circularization efficiency was measured at different concentrations of transforming DNA (*ura4*$^+$ PCR product or REP4[*ura4*$^+$]) in wild-type (PN559) and *rad50*Δ (KT120) cells. WT, wild type.

show reduced circularization efficiency as compared to *pku70*Δ cells (Figure 1B). The drastic reduction in the number of Ura$^+$ colonies obtained in NHEJ-deficient strains further argues against a high frequency of *ura4*$^+$ DNA integration into the yeast genome.

Next, repair mechanisms involved in *ura4*$^+$ circularization (NHEJ or MMEJ) were classified according to the extent of microhomology at *ura4*$^+$ junctions. Overlapping sequences ≥5 bp and composing at least 4 bp of perfect microhomology were classified as MMEJ-mediated intramolecular ligations of *ura4*$^+$ and overlap <5 bp as NHEJ-dependent ligations. Following these criteria, 93% (43/46) of *ura4*$^+$ circularizations were mediated through NHEJ in wild-type cells (Figure 2A), and nucleotide loss at junctions was detected in 83% of the repair events (Figure 2, A and B). Deletion of the *rad50*$^+$ gene did not affect significantly the extent of nucleotide deletion at repair junctions and NHEJ produced 81% (57/70) of the *ura4*$^+$ circles (Figure 2, A and B). In *pku70*Δ cells, nucleotide deletion was observed at all junctions and MMEJ accounted for 92% (24/26) of the repair events. MMEJ frequency was reduced to 71% (10/14) in *lig4*Δ cells, suggesting that another ligase may be involved in *pku70*$^+$-dependent NHEJ in *S. pombe*. The situation observed in *lig4*Δ *pku70*Δ cells was similar to the one observed in *pku70*Δ cells in agreement with the involvement of *pku70*$^+$ and *lig4*$^+$ genes in the same NHEJ pathway (Figure 2, A and B). Hence, PCR-amplified *ura4*$^+$ DNA seems to be a good substrate to monitor EC DSB repair in fission yeast, allowing the study of both NHEJ and MMEJ repair pathways.

High frequency of mtDNA insertion at extrachromosomal DSBs: A striking feature of the *ura4*$^+$ EC DSB repair assay was the presence of DNA inserts in 28% (61/221) and 11% (7/61) of the circular *ura4*$^+$ molecules isolated from wild-type and *rhp51*Δ cells, respectively (Figures 1A and 3A). All DNA inserts consisted of fission yeast mtDNA exclusively and included 19% (7/36) and 28% (2/7) of multiple mtDNA insertions in wild-type and *rhp51*Δ cells, respectively (Table 2). mtDNA capture at EC DSBs was not dependent upon DSB end sequence as similar capture frequency was observed with *ura4*$^+$ DNA flanked by 20-bp-long random sequences (data not shown). mtDNA capture also was not restricted to PCR-amplified repair substrate as a similar mtDNA insertion frequency (24%) was observed at repair junctions of yeast cells transformed with *Eco*RI-linearized pUC18::*ura4*$^+$ plasmid (Figure 3B). mtDNA insert size ranged from 83 to 4004 bp (Table 2). However, longer mtDNA inserts may not have been detected (1 min 30 sec elongation time for PCR). In both strains, homologies of 0–3 bp were detected at the mtDNA-*ura4*$^+$ junctions, a hallmark of NHEJ-mediated ligations. Accordingly, mtDNA was never found at repair junctions in *pku70*Δ (0/229), *lig4*Δ (0/372), and *lig4*Δ *pku70*Δ (0/158) NHEJ-deficient strains (Figure 3A). Interestingly, mtDNA also was not detected in the 215

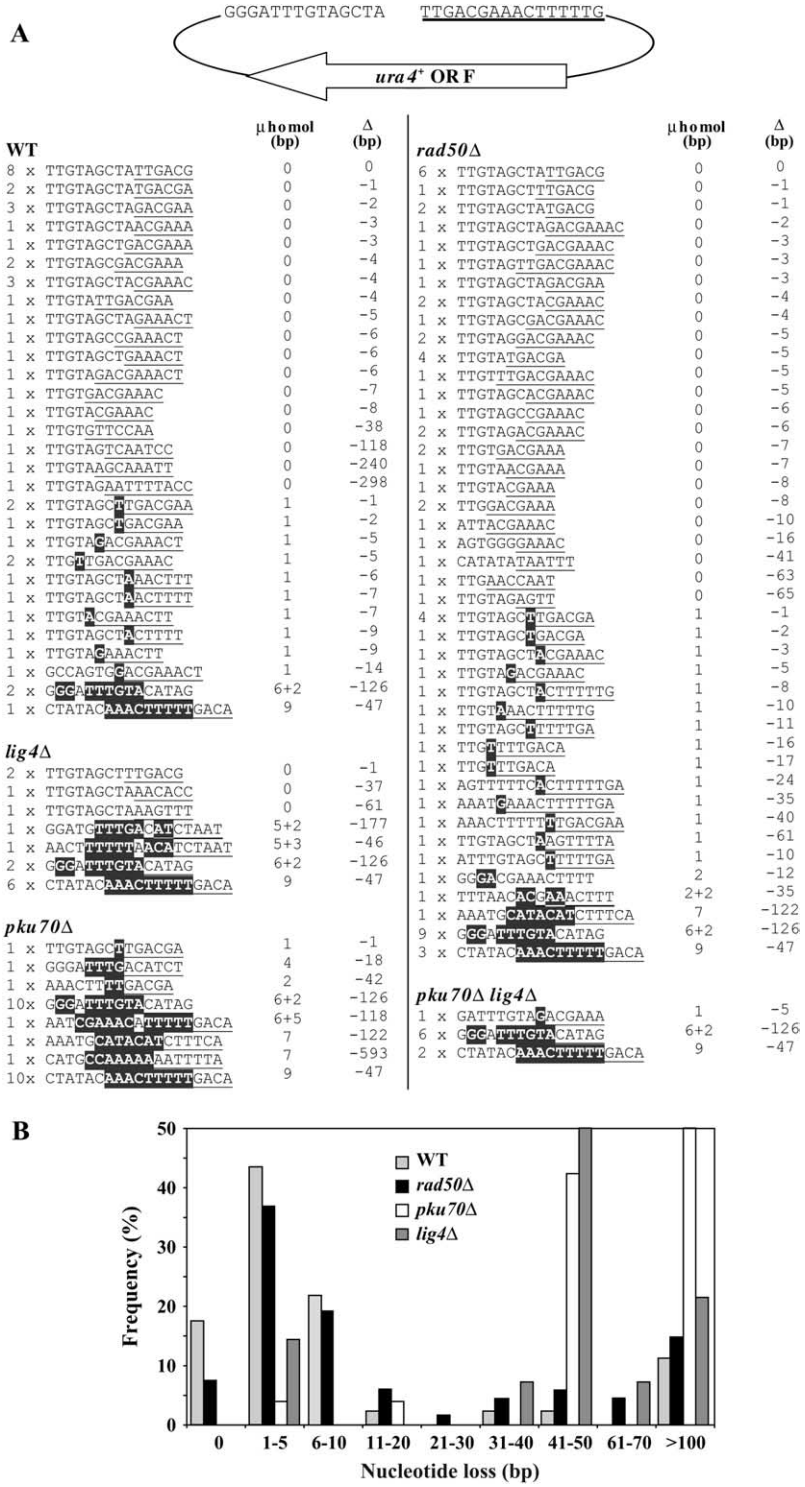

FIGURE 2.—Repair junctions in *ura4*$^+$ circles. (A) Nucleotide sequence of *ura4*$^+$ repair junctions. Overlapping residues at junctions are shaded. The accumulated nucleotide loss (5′ + 3′) is given under "Δ." (B) Distribution of accumulated nucleotide loss at repair junctions.

repair events analyzed in the *rad50*Δ background (Figure 3A), reflecting either intermolecular ligation deficiency of the strain or the absence/reduction of mtDNA fragments in the nucleus of *rad50*Δ cells.

Intermolecular ligation deficiency of *rad50*Δ cells: To investigate the ability of *rad50*Δ cells to ligate two pieces of DNA together (intermolecular ligation), I next measured the efficiency of mtDNA capture at EC DSBs in cotransformation experiments (Figure 4A). Exponentially growing *rad50*Δ cells were cotransformed with 2 μg *ura4*$^+$ DNA and 2 μg 600-bp PCR-amplified *S. pombe* mtDNA fragment (1:3 molar ratio). Although the mtDNA fragment was detected in 53% (9/17) of the *ura4*$^+$ circles produced in wild-type cells, the frequency of mtDNA ligation to *ura4*$^+$ was decreased by fourfold, down to 13% (5/38), in *rad50*Δ cells, suggesting that Rad50p is indeed required for efficient intermolecular ligation. However, loss of Lig4p had a more drastic effect

A

	PCR positive ura+ colonies	*ura4*+ circles with insert	Inserts with *S. pombe* mtDNA
WT	**70%** (221/317)	**28%** (61/221)	**100%** (61/61)
***rhp51*Δ**	**68%** (61/90)	**11%** (7/61)	**100%** (7/7)
***rad50*Δ**	**82%** (215/261)	**0%** (0/215)	-
***lig4*Δ**	**91%** (372/410)	**0%** (0/372)	-
***pku70*Δ**	**88%** (229/360)	**0%** (0/229)	-
***lig4*Δ*pku70*Δ**	**90%** (158/176)	**0%** (0/158)	-

B

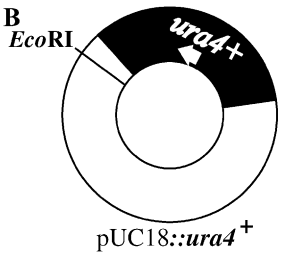

PCR positive ura+ colonies	84% (42/50)
pUC18::*ura4*+ with insert	24% (10/42)
Inserts with *S. pombe* mtDNA	100% (10/10)

FIGURE 3.—mtDNA capture at EC DSBs. PCR analysis of *ura4*$^+$ repair junctions in Ura$^+$ colonies obtained either after transformation of exponentially growing wild-type (PN559), *rhp51*Δ (PN2490), *rad50*Δ (KT120), *lig4*Δ (AD459), *pku70*Δ (PN3773), and *lig4*Δ*pku70*Δ (AD462) cells with 2 μg PCR-amplified *ura4*$^+$ DNA (A) or after transformation of wild-type cells with 1 μg *Eco*RI-linearized pUC18::*ura4*$^+$ plasmid (B). WT, wild type.

on intermolecular ligation since mtDNA was absent from the 23 *ura4*$^+$ circles analyzed in *lig4*Δ cells. These data suggest that the fission yeast Rad32p/Rad50p/Nbs1p complex is required for efficient intermolecular ligation.

Increased capture of mtDNA fragments in stationary phase: Next, to test whether endogenously produced mtDNA fragments may be inserted at EC DSBs in *rad50*Δ cells, I searched for growth conditions that would increase mtDNA capture frequency, thereby circumventing the intermolecular ligation defect. Because of increased superoxide production in yeast cells grown to stationary phase (after the diauxic shift) and because of the proximity of mtDNA to superoxide production sites, the lack of histones, and the reduced repair activity, mtDNA may be damaged, and possibly more fragmented, in such cells (LONGO *et al.* 1999). Moreover, stationary phase may increase the rate of mtDNA transfer to the nucleus through increased mitochondria degradation (TAKESHIGE *et al.* 1992). Therefore, I tested whether capture of endogenously produced mtDNA fragments may be detected at EC DSBs of *rad50*Δ cells grown to stationary phase.

Accordingly, I found that transformation of stationary-phase wild-type cells with 2 μg *ura4*$^+$ PCR product increased the frequency of mtDNA insertions in *ura4*$^+$ circles to 73% (16/22), compared to 28% (61/221) in exponentially grown wild-type cells and multiple insertions amounted to 56% (9/16) of the events, with up to seven pieces of mtDNA ligated to a single *ura4*$^+$ molecule (Figure 4, C and D, and Table 2). Under these conditions, mtDNA insertions were observed in 31% (9/29) of the *ura4*$^+$ circles isolated from *rad50*Δ cells, thereby demonstrating that, at least in stationary phase, mtDNA fragments are available for ligation to *ura4*$^+$ in *rad50*Δ cells (Figure 4C and Table 2). However, multiple insertions of mtDNA pieces were much less abundant than in wild-type cells (Figure 4D), further supporting the intermolecular ligation deficiency of *rad50*Δ cells. Mitochondria-targeted GFP fluorescence revealed that the transition to stationary phase had caused drastic changes, shifting the pattern from tubular networks to punctate mitochondrial structures (Figure 4B), as reported in budding yeast (VISSER *et al.* 1995). Strikingly, mitochondria from glucose-starved cells were enriched at the cell periphery and around the nucleus, raising the interesting hypothesis that this may help the transfer of mtDNA fragments into the nucleus.

Screen for higher eukaryotic DNA sequences captured at DSBs: Although capture of mtDNA at experimentally induced DSBs had been previously reported only in *S. cerevisiae*, a few studies in plant and mammalian cells have reported the insertion of genomic DNA (GORBUNOVA and LEVY 1997; SARGENT *et al.* 1997; SALOMON and PUCHTA 1998; LITTLE and CHARTRAND 2004), including microsatellite sequences (LIANG *et al.* 1998; LIN and WALDMAN 2001a). Using the fission yeast EC DSB repair assay, I screened for higher eukaryotic DNA sequences that may be preferentially captured at DSBs. This was achieved by cotransforming 2×10^8 fission yeast cells with 2 μg *ura4*$^+$ DNA and 50 μg genomic DNA from either salmon sperm or 293 human embryonic kidney cells, knowing that 50 μg human genomic DNA represent ~10^7 nuclear genomes (and presumably a similar amount of salmon nuclear genomes). Cotransformation of wild-type cells with *ura4*$^+$ PCR product and sheared salmon sperm DNA yielded ~30% (42/141) *ura4*$^+$ circles with inserted DNA (Figure 5A). Frequency of yeast mtDNA in the inserts was reduced to 13% (Figure 5B). Interestingly, salmon microsatellite DNA fragments (15–~500 bp), mainly $(GT)_n$ dinucleotide repeats, amounted to 21% of the *ura4*$^+$ circle inserts and, in two cases, two tracts of dinucleotide repeats were present within the same circular molecule (Figure 5C and supplemental data I at http://www.genetics.org/supplemental/). Since $(GT)_n$ dinucleotide repeats of >38 bp long are absent from the *S. pombe* genome, the long microsatellite DNA inserts must come from the cotransforming salmon DNA. Nonmicrosatellite repetitive DNA fragments of ~100–~350 bp, including ribosomal DNA, represented another 39% of the inserts in wild-type cells (Figure 5C). Similar distribution of microsatellite and nonmicrosatellite salmon repetitive DNA was observed in *rhp51*Δ inserts (Figure 5C). However, no capture of salmon sperm DNA had occurred at the 96 repair junctions analyzed in *rad50*Δ cells (Figure 5A). This may be related to the intermolecular deficiency of the strain and/or to the inability of *rad50*Δ cells to excise a piece of DNA from the bulk of salmon

TABLE 2

Examples of mitochondrial DNA inserts

Insert length (bp)	Position on mitochondrial genome
	WT exponential
4004	9082–13085
3148	15308–12161
2811	14128–16938
2465	10006–7542
2333	16207–18539
1840	8856–7017
1322	7606–6285
1182	7402–8583
994	18752–404
878	5665–6542
792	5976–5185
767	5665–6431
760	6515–5756
732	10018–10749
718	7075–7792
687	5214–4528
669	7870–7202
620	5879–6498
559	15533–14975
537	5980–6516
521	14925–14425
435	6015–5581
429	6887–7315
400	2869–2470
400	2470–2869
355	6217–6571
348	7947–7600
320	15081–14762
159	14041–13883
936, 111	13896–14831, 314–424
217, 457	18678–18462, 11770–12226
543, 285	16658–17200, 19020–19304
189, 167	15503–15315, 6329–6163
92, 213	4675–4766, 12198–12410
126, 207, 87	5834–5959, 15912–16118, 15781–15867
115, 102, 160, 83	5579–5465, 17505–17404, 14264–14105, 17754–17836
	*rhp51*Δ exponential
868	17612–18479
529	14606–15134
296	16306–16011
244	19337–239
178	4965–4788
773, 806	3698–4470, 14301–15106
295, 298	13088–12794, 13607–13904
	WT stationary
1045	13728–14772
917	14599–15515
879	16060–16937
485	13083–12599
361	5661–6021
359	7683–8041
322	14587–14908
183, 451	16224–16041, 5649–6099
84, 81	1057–1140, 6199–6279
112, 80, 210	4757–4646, 4718–4639, 8988–8779
219, 124, 117	4757–4539, 18245–18368, 18992–18876
201, 215, 815	3865–3665, 1855–2069, 7277–8041
216, 178, 115, 140	12321–12106, 4951–4774, 13987–14101, 5440–5579
152, 156, 106, 108, 114	6546–6697, 7710–7865, 18723–18828, 6654–6761, 8800–8687
176, 86, 117, 409, 173, 437	5417–5242, 7683–7598, 8451–8567, 3945–4353, 6157–6329, 5625–6061
421, 138, 98, 367, 87, 95, 83	8634–9054, 15071–14934, 5885–5788, 17138–16772, 10774–10688, 9475–9381, 1027–945
	*rad50*Δ stationary
598	14642–15239
424	7592–8015
406	16525–16126
371	1777–2147
331	6524–6194
297	6119–5823
164	11401–11564
60	16522–16463
78, 248	7626–7703, 6569–6322

(*continued*)

genomic DNA to fill in EC DSBs. Similarly, none of the *ura4*$^+$ circular molecules analyzed in either *lig4*Δ (0/74) or *pku70*Δ (0/71) cells had captured salmon DNA (Figure 5A). In a second experiment, wild-type fission yeast cells were cotransformed with 2 μg *ura4*$^+$ PCR product and 50 μg human genomic DNA. Similarly, human genomic DNA competed with endogenous yeast mtDNA fragments for ligation to the *ura4*$^+$ gene, reducing the frequency of mtDNA to ~11% (1/9) of the inserts (Figure 5B). Here also $(GT)_n$ microsatellite DNA was recovered at the insert-*ura4*$^+$ junction in one of the clones analyzed (Figure 5, D and E). The remaining inserts comprised other kinds of human repetitive DNA (Figure 5D), which, because of their abundancy in the human genome (repetitive DNA accounts for at least 50% of the total genomic content according to Lander *et al.* 2001), may not represent preferred substrates for NHEJ.

MMEJ-mediated intermolecular ligation in NHEJ-deficient cells: It is well established that NHEJ machinery is required for efficient ligation of two pieces of DNA. Here, I tested whether MMEJ may also drive the insertion of a DNA fragment into *ura4*$^+$ circles.

Two micrograms of a 267-bp piece of PCR-amplified human genomic DNA (hDNA) flanked by stretches of 8 bp of homology to *ura4*$^+$ 5′- and 3′-ends was introduced into yeast together with 2 μg of *ura4*$^+$ DNA (6:1 molar ratio) (Figure 6A). Microhomology at the 5′-end of

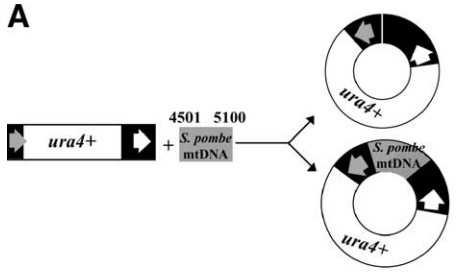

WT	*rad50*Δ	*lig4*Δ
47% (8)	87% (33)	100% (23)
53% (9)	13% (5)	0%

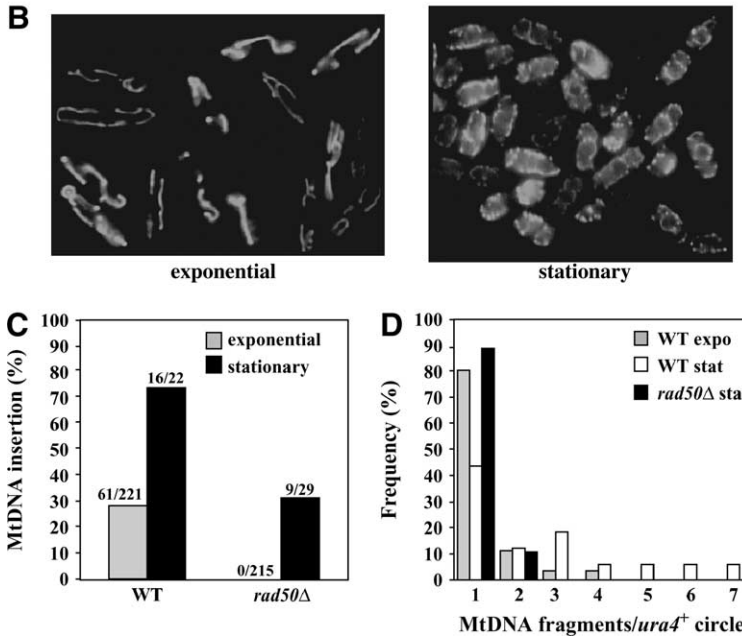

FIGURE 4.—Intermolecular ligation deficiency of *rad50*Δ cells. (A) mtDNA insertion frequencies after cotransformation of exponentially growing wild-type (PN559), *rad50*Δ (KT120), and *lig4*Δ (AD459) cells with PCR-amplified *ura4*$^+$ and mtDNA fragments (1:3 molar ratio). The number of *ura4*$^+$ molecules analyzed is shown in parentheses. Data are the result of at least two independent yeast transformations. (B) Live observation of mitochondria morphology using the *atp3-GFP* fusion in wild-type cells grown either exponentially or to stationary phase in glucose medium. (C) Insertion frequency of mtDNA fragments in *ura4*$^+$ circles recovered from wild-type and *rad50*Δ cells grown to either exponential or stationary phase. The number of *ura4*$^+$ circular molecules analyzed is given at the top of each bar. (D) Number of mtDNA pieces ligated to a single *ura4*$^+$ molecule in wild-type and *rad50*Δ cells grown under both conditions. WT, wild type.

hDNA corresponded to the very last 8 bp of the *ura4*$^+$ 3′-end while the microhomologous region between the hDNA 3′-end and *ura4*$^+$ lay 3 bp away from the 5′-end of *ura4*$^+$, thereby mimicking a MMEJ substrate. In wild-type cells, the hDNA fragment was inserted in 68% (32/47) of *ura4*$^+$ circles and the insertion frequency was reduced to 28% (14/50) in the *rad50*Δ mutant (Figure 6C). In cells lacking either *lig4*$^+$ or *pku70*$^+$ or both genes, although the number of Ura$^+$ colonies recovered after cotransformation was low (Figure 6B), the frequency of hDNA insertion was high, amounting to, respectively, 70% (23/33), 55% (18/33), and 74% (14/19) of the circular molecules (Figure 6C). Hence, it appears that, under the assay conditions, the relative cellular efficiency of intermolecular ligation (hDNA insertion into *ura4*$^+$) *vs.* intramolecular ligation (*ura4*$^+$ circularization without hDNA insertion) was affected by the loss of the Rad32p/Rad50p/Nbs1p complex but was not dependent on the Lig4p/Pku70p NHEJ machinery.

The mechanism involved in hDNA insertion was identified after sequencing of the junctions between hDNA and *ura4*$^+$. The absence of an 8-bp overlap at circle junctions in both wild-type (0/32) and *rhp51*Δ (0/7) cells suggests that NHEJ, and not MMEJ was involved in 100% of the insertions (Figure 6D). However, in *lig4*Δ, *pku70*Δ, and *lig4*Δ*pku70*Δ cells, insertion of hDNA was probably exclusively mediated through MMEJ as 8-bp overlaps were detected at all junctions (23/23, 18/18, and 14/14, respectively) (Figure 6D). Interestingly, MMEJ-mediated insertions of hDNA were also detected in 29% (4/14) of insertional events in *rad50*Δ cells. Taking into account the frequency of hDNA insertion and the number of Ura$^+$ colonies obtained after transformation of *rad50*Δ and *lig4*Δ cells, data suggest that, under the experimental conditions, the number of MMEJ-mediated intermolecular ligations may be similar in *rad50*Δ and *lig4*Δ backgrounds, amounting to an average of 70 events/yeast transformation, which represents a frequency of $\sim 3.5 \times 10^{-7}$/2 μg of each transforming DNA.

As expected, the efficiency of hDNA insertion mediated through long stretches of homology was very high in all yeast backgrounds tested (Figure 6, A–D). Indeed, cotransformation of yeast with 2 μg *ura4*$^+$ DNA and 2 μg hDNA flanked by 205 bp (5′) and 401 bp (3′) of homology to *ura4*$^+$ (1:2 molar ratio) yielded a high number of Ura$^+$ colonies, and the hDNA insert was present in 100% of the *ura4*$^+$ circles formed (Figure 6, A–D). The presence of the hDNA insert in all *ura4*$^+$ molecules isolated from *rhp51*Δ cells suggests that yeast relied on

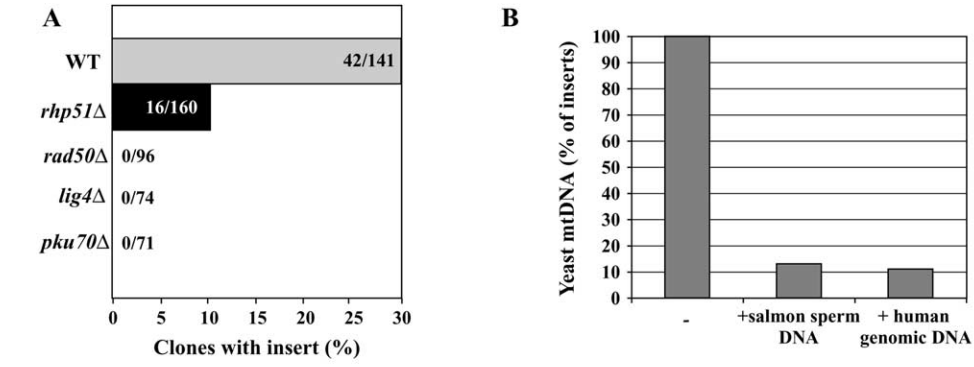

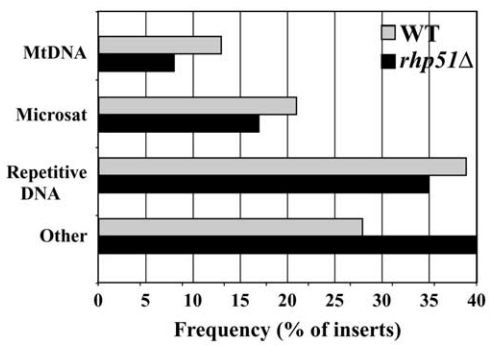

D

Clone	Insert length	Position on human chromosomes	DNA type
1	2.5 kb	8q21	repeat region (L1MDa)
2	1.95 kb	21q22.2	repeat region
3	1.3 kb	8q23	repeat region (L1MD2)
4	887 bp	18p11.3	repeat region + (GT)17
5	717 bp	4q35	repeat region (AT rich)
6	738 bp	12p11	repeat region (AluSx, MIR)
7	250 bp	centromere of chr. 13	minisatellite
8	222 bp	4q22	repeat region (AT rich)

E Clone 4

ATTTGTAGCTAGAAAATATCTAAACGT....824 bp....ATATATATATGTGTGTGTGTGTGTGTGTGTGTGTATGTGTGTGGACGAAAC

FIGURE 5.—Capture of DNA fragments from higher eukaryotes at fission yeast DSBs. (A) Frequency of *ura4*$^+$ molecules with inserted DNA after transformation of exponentially growing wild-type (PN559), *rhp51*Δ (PN2490), *rad50*Δ (KT120), *lig4*Δ (AD459), and *pku70*Δ (PN3773) cells with 2 μg *ura4*$^+$ DNA and 50 μg sheared salmon sperm DNA. The number of *ura4*$^+$ molecules analyzed is shown on the bars. Three to six independent transformations were performed for each strain. (B) Frequency of fission yeast mtDNA in *ura4*$^+$ inserts recovered from cells transformed with 2 μg *ura4*$^+$ DNA only (−) and either 50 μg salmon sperm DNA or 50 μg human genomic DNA. (C) Inserts recovered from wild-type and *rhp51*Δ cells were classified as follows: fission yeast mtDNA, salmon microsatellite DNA, salmon repetitive DNA including ribosomal DNA, and other salmon DNA sequences. (D) Characteristics of human genomic DNA inserts recovered in the assay. (E) Insert of clone 4 showing the presence of $(GT)_{17}$ repeats at the 3′ junction. WT, wild type.

the *RAD51*-independent single-strand-annealing (SSA) mechanism of HR and not on *RAD51*-dependent gene conversion for insertion of hDNA with long stretches of homology. In the *lig4*Δ background, the frequency of SSA-driven insertions of hDNA was 5×10^{-4}, representing a 1500-fold increase in frequency compared to MMEJ ($5 \times 10^{-4}/3.5 \times 10^{-7}$). In wild-type cells, SSA-dependent insertion of hDNA was ~30-fold more frequent than NHEJ under the assay conditions ($5 \times 10^{-4}/1.5 \times 10^{-5}$).

All together, the PCR assay provided evidence that MMEJ-dependent intermolecular ligation is feasible, but not very efficient, in fission yeast. However, in the presence of both the Rad32p/Rad50p/Nbs1p complex and the Lig4p/Pku70p NHEJ machinery, cells relied exclusively on the more efficient NHEJ pathway for ligation of hDNA to *ura4*$^+$. Both MMEJ and NHEJ pathways of DNA insertion were less efficient than SSA.

DISCUSSION

New assay to monitor extrachromosomal DSB repair in *S. pombe*: This work validated the use of PCR-amplified *ura4*$^+$ DNA as substrate for the study of EC DSB repair in fission yeast as the extremities of *ura4*$^+$ linear DNA were recognized as DSBs and subjected to either NHEJ or MMEJ to produce circular *ura4*$^+$ molecules. In wild-type cells, nucleotide loss was observed at 83% of repair junctions in agreement with previous studies in fission yeast reporting the formation of 15–40% accurate junctions during NHEJ-mediated repair of linearized plasmids (WILSON *et al.* 1999; MANOLIS *et al.* 2001). Deletion of the *rhp51*$^+$ gene did not impair EC DSB repair efficiency. However, *ura4*$^+$ circularization efficiency was drastically reduced in *lig4*Δ and *pku70*Δ cells. No accurate junction was detected in the latter strains since ligation had mainly occurred at microhomologous regions that were buried within the *ura4*$^+$ DNA. Sequence overlaps were often imperfect and had

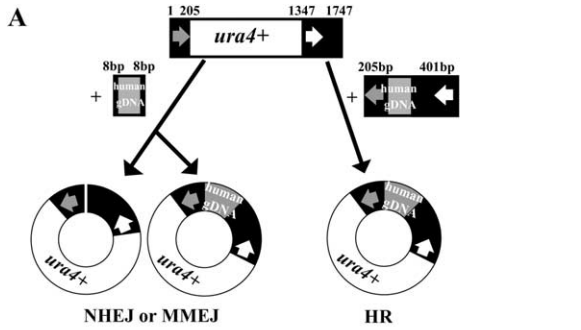

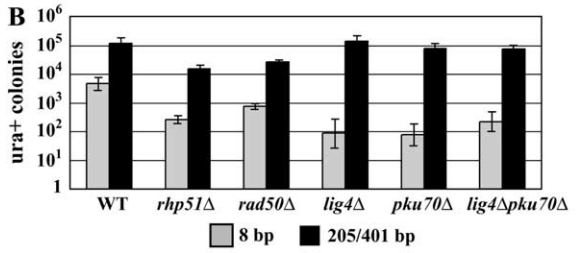

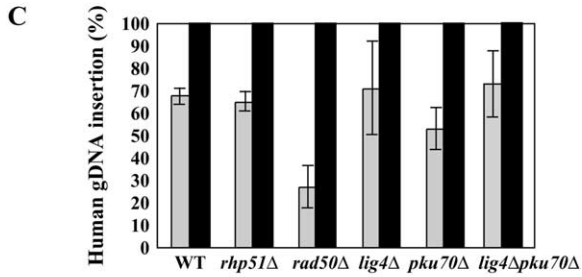

D

	human gDNA with microhomologies		human gDNA with long homologies
	NHEJ	MMEJ	HR
WT	100% (32)	0	100% (8)
*rhp51*Δ	100% (7)	0	100% (8)
*rad50*Δ	71% (10)	29% (4)	100% (10)
*lig4*Δ	0	100% (23)	100% (9)
*pku70*Δ	0	100% (18)	100% (9)
*lig4*Δ*pku70*Δ	0	100% (14)	100% (8)

Figure 6.—MMEJ-mediated intermolecular ligation in NHEJ-deficient cells. (A) Exponentially growing cells were cotransformed with *ura4*$^+$ DNA and hDNA flanked by either microhomologous (8 bp) or homologous (205 and 401 bp) sequences to 5′- and 3′-ends of *ura4*$^+$ DNA. (B) Number of Ura$^+$ colonies obtained after independent transformations of wild-type (PN559), *rhp51*Δ (PN2490), *rad50*Δ (KT120), *lig4*Δ (AD459), *pku70*Δ (PN3773), and *lig4*Δ*pku70*Δ (AD462) cells with 2 μg *ura4*$^+$ DNA and either 2 μg microhomologous hDNA or 2 μg homologous hDNA. (C) Insertion frequency of both hDNA types. (D) Repair pathway for hDNA insertion in *ura4*$^+$ circles based on overlapping sequences at junctions. For cotransformation with microhomologous hDNA, insertions were classified under MMEJ if the 8 bp overlapped at junctions. The number of sequenced inserts is shown in parentheses. WT, wild type.

a mean length of 8.8 bp (5–12 bp), a value close to the mean length of 11.2 bp (5–20 bp) reported at budding yeast overlapping MMEJ junctions (Kramer *et al.* 1994; Manivasakam *et al.* 1995; Boulton and Jackson 1996; Yu and Gabriel 1999; Ma *et al.* 2003) and similar to the 8-bp overlap found at NHEJ-independent repair junctions in human bladder cancer cell-free extracts (Bentley *et al.* 2004). Under the assay conditions, absence of the functional fission yeast Mre11 complex affected neither *ura4*$^+$ intramolecular ligation efficiency nor the extent of nucleotide loss at repair junctions in agreement with Manolis *et al.* (2001). However, the budding yeast Mre11 complex is required for efficient end-joining of DSBs (Schiestl *et al.* 1994; Moore and Haber 1996; Boulton and Jackson 1998; Ma *et al.* 2003).

On the other hand, this study confirmed that fission yeast NHEJ efficiently repairs EC DSBs with noncohesive ends, unlike budding yeast for which Boulton and Jackson (1996) reported a 50-fold decrease in the efficiency of *YKU70*-dependent repair of blunt ends.

Insertion of mtDNA at EC DSBs: mtDNA insertions were detected in 28% of the *ura4*$^+$ circles recovered from exponentially growing wild-type cells and included 19% of multiple insertions (two to four pieces). mtDNA insertions were also detected in *rhp51*Δ cells, but not in NHEJ-deficient *lig4*Δ or *pku70*Δ strains. mtDNA also was not recovered from *rad50*Δ *ura4*$^+$ circles probably because, in the absence of the Mre11 complex end-bridging activity (Anderson *et al.* 2001; Chen *et al.* 2001), the local concentration of *ura4*$^+$ and mtDNA molecules is not high enough, reducing intermolecular ligation efficiency. Cotransformation of yeast with *ura4*$^+$ DNA and a PCR-amplified mtDNA fragment in a 1:3 molar ratio probably increased the intracellular mtDNA fragment concentration in *rad50*Δ cells, resulting in a capture frequency of 13%. However, capture of a cotransformed mtDNA fragment was four times more efficient in wild-type cells compared to *rad50*Δ cells, providing direct evidence for reduced intermolecular efficiency in Mre11-deficient cells. Hence, *rad50*Δ cells may not be able to capture endogenous mtDNA fragments if their cellular concentration is below a threshold value required for intermolecular ligation.

Growing cells to stationary phase provided more evidence in favor of reduced intermolecular ligation efficiency in *rad50*Δ cells. Indeed, although 73% of *ura4*$^+$ circles had captured endogenous mtDNA in stationary-phase wild-type cells, the capture frequency was reduced to 31% in *rad50*Δ cells and multiple insertional events were much less frequent than in wild-type cells. Southern blot analysis did not reveal significant differences in the amount of mtDNA in wild-type and *rad50*Δ post-diauxic *vs.* exponentially growing cells (data not shown). However, the higher production of superoxide in mitochondria from stationary-phase yeast (Longo *et al.* 1999) may increase mtDNA fragmentation, given the lack of histones and the reduced repair activity in mitochondria. In addition, mitochondria-containing vacuolar autophagic bodies accumulate in budding yeast stationary phase (Takeshige *et al.* 1992), providing a mechanism

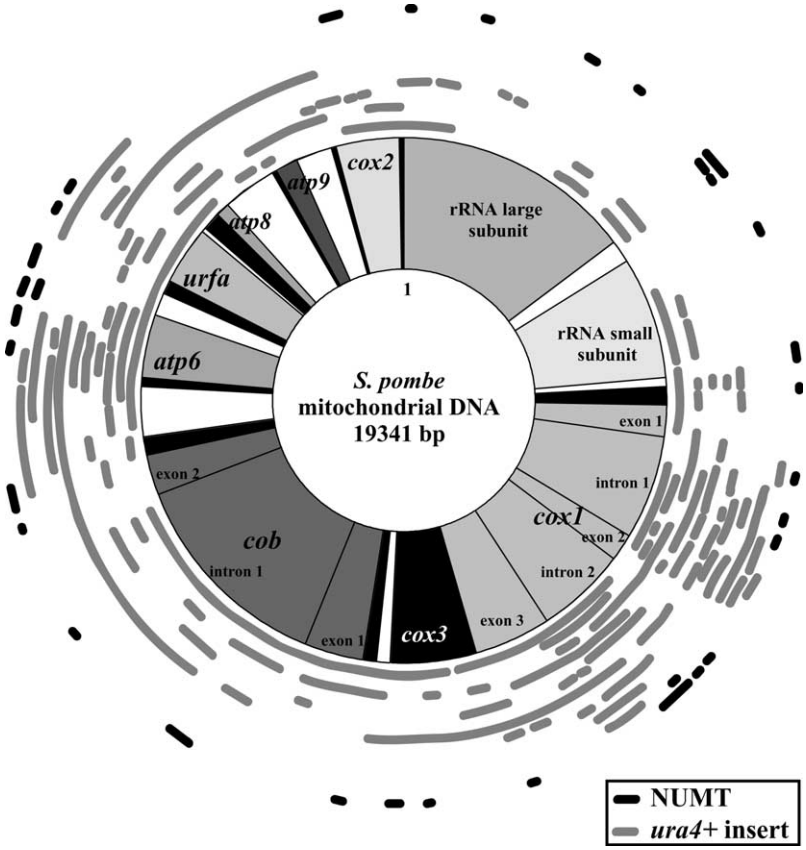

FIGURE 7.—*S. pombe* NUMTs. Comparison of fission yeast mitochondrial and nuclear genomes revealed the presence of 33 putative NUMTs (black lines). The position of NUMTs on the *S. pombe* mitochondrial genomic map is compared to the position of mtDNA fragments recovered in *ura4*$^+$ circles in this study (gray lines).

for increased release of mtDNA molecules in the cytoplasm (CAMPBELL and THORSNESS 1998). Alternatively, increased mtDNA capture frequency may be due to enhanced NHEJ efficiency in glucose-starved cells as suggested by studies of budding yeast (KARATHANASIS and WILSON 2002; HEIDENREICH *et al.* 2003). Finally, it should be emphasized that yeast cells grown to stationary phase resemble most of the cells from multicellular organisms since (1) most energy comes from mitochondrial respiration and (2) cells have exited from the cell cycle; *i.e.*, they have entered the G_0 phase.

Capture of mtDNA fragments at EC DSBs has been previously reported in *S. cerevisiae* and amounted to ~10% of the repair events (SCHIESTL *et al.* 1993). One hypothesis to explain the surprisingly high frequency of mtDNA insertion at EC DSBs in either budding yeast or fission yeast cells may be that the transformation procedure facilitates mtDNA fragment transfer to the nucleus as previously suggested (SCHIESTL *et al.* 1993). Alternatively, the ligation of mtDNA to *ura4*$^+$ DNA may take place in the cytoplasm prior to transfer into the nucleus as different studies in higher eukaryotic cells reported a cytoplasmic localization of both the Mre11 complex and the Ku proteins under certain circumstances (ZHU *et al.* 2001; KOIKE 2002; SENO and DYNLACHT 2004). However, translocation of these DNA repair proteins to the cytoplasm is rather viewed as a regulatory mechanism that inhibits nuclear NHEJ and it remains to be established whether cytoplasmic DNA repair exists. Nevertheless, mtDNA capture at chromosomal DSBs has been clearly established in budding yeast experimental models, supporting the existence of mtDNA transfer to the nucleus (RICCHETTI *et al.* 1999; YU and GABRIEL 1999, 2003). Consistent with this view, the *de novo* chromosomal integration of mtDNA associated with Pallister-Hall syndrome in a patient exposed to Chernobyl radiations may be the consequence of NHEJ-mediated repair of radiation-induced DSBs (TURNER *et al.* 2003). Human mtDNA insertion has also been detected at the breakpoint junction of a reciprocal constitutive translocation (WILLETT-BROZICK *et al.* 2001). Genome sequence analysis of budding yeast (RICCHETTI *et al.* 1999), human (MOURIER *et al.* 2001; TOURMEN *et al.* 2002; WOISCHNIK and MORAES 2002; RICCHETTI *et al.* 2004), and various plant species (RICHLY and LEISTER 2004) provided more evidence in favor of nuclear genome colonization by mtDNA. Depending on the threshold value used for the BLAST search, 211–612 human NUMTs (up to 14,654 bp long) and 34 budding yeast NUMTs (22–230 bp long) were detected. *S. pombe* nuclear genome analysis revealed the presence of 33 NUMTs (22–358 bp long), mainly in intergenic regions and spread over three chromosomes (Figure 7 and supplemental data II at http://www.genetics.org/supplemental/). The presence of two to three NUMTs at some genomic loci suggests that multiple insertions of mtDNA fragments also occurred during *S. pombe* genome evolution. There was no obvious bias for the

nature of colonizing mtDNA although three NUMTs and two identical 400-bp inserts recovered in independent yeast transformations are within the 3′-end region of the rRNA large subunit gene (Figure 7). On the other hand, the *ura4*$^+$ circle mtDNA inserts were enriched in DNA from *cox1*$^+$ gene introns (Figure 7) in agreement with the presence of *COX1* intronic DNA in four of nine mtDNA inserts recovered at budding yeast experimental chromosomal DSBs (Ricchetti *et al.* 1999).

This study revealed that NHEJ-mediated mtDNA insertion at EC DSBs occurs in fission yeast and provides a tool for understanding the mechanisms of production and/or transfer of mtDNA fragments in the nucleus.

Microsatellite DNA is a good substrate for NHEJ in fission yeast: Microsatellite DNA from higher eukaryotes was preferentially captured at EC DSBs in wild-type and *rhp51*Δ fission yeast cells. Dinucleotide repeats (15–~500 bp long) were found in 21% of the *ura4*$^+$ inserts recovered after cotransformation with salmon DNA and the $(CCG)_8$ trinucleotide repeat was detected at one of the repair junctions. Because dinucleotide repeats amount to only ~0.25% of the total genomic DNA in vertebrates (Tóth *et al.* 2000), their capture at DSBs may be as much as 100-fold more frequent than expected. $(GT)_n$ repeats, the most abundant dinucleotide repeats in vertebrates (60% of them) (Tóth *et al.* 2000), accounted for 67% of the microsatellite DNA inserts. In mammalian cells, two previous studies have reported the insertion of microsatellite DNA at DSBs (Liang *et al.* 1998; Lin and Waldman 2001a). Moreover, Boehm *et al.* (1989) reported the presence of $(GT)_n$ tracts (62–~800 bp long) at the breakpoint of three different human lymphoid tumor-specific translocations, one of them involving the T-cell receptor β-gene. Hence, it appears that the preferential patching of DSBs with microsatellite DNA may be conserved in eukaryotic cells, validating yeast as a model for understanding the molecular basis of that preference. As previously suggested (Liang *et al.* 1998), DSB repair may provide a mechanism for the spreading of microsatellite DNA in the genome. Hence, DSB repair may possibly be associated with an increased risk of repeat-DNA expansion-associated genetic diseases, such as Huntington's disease $[(AGC)_n]$, Friedreich's ataxia $[(AAG)_n]$ (Richards and Sutherland 1997), or $(AT)_n$ expansions associated with autoimmune disorders (Huang *et al.* 2000).

MMEJ-dependent intermolecular ligation: Although the NHEJ machinery has been shown to drive insertion of DNA fragments at budding yeast DSBs (Yu and Gabriel 2003), MMEJ-mediated insertions have not been reported so far. This study provided evidence that, in the absence of Pku70p/Lig4p, MMEJ is able to mediate the insertion of microhomologous DNA substrates at EC DSBs, albeit with low efficiency. However, in wild-type cells, NHEJ was exclusively responsible for microhomologous DNA substrate insertion. In *rad50*Δ cells, the DNA substrate capture frequency was decreased in agreement with the intermolecular ligation deficiency, and MMEJ-mediated insertions accounted for nearly 30% of the insertional events. Therefore, in the absence of the Rad32p/Rad50p/Nbs1p complex, the processing of DSBs required for annealing of complementary nucleotides in MMEJ may have more time to proceed, changing the competition rules between NHEJ and MMEJ. Finally, the data suggested that SSA-driven insertions of DNA with long stretches of homology have an increased efficiency of 30- and 1500-fold compared to NHEJ- and MMEJ-dependent insertions, respectively.

In summary, a new simple assay for EC DSB repair, based on PCR-amplified DNA substrate, was developed in fission yeast. The flexibility in the design of primer sequences offers a tool to investigate the repair of various DSB end sequences. The assay demonstrated a role for the fission yeast Rad32p/Rad50p/Nbs1p complex in promoting intermolecular ligation and unraveled the capture of fission yeast mtDNA and microsatellite DNA from higher eukaryotes at EC DSBs in *S. pombe*. The conservation of the NHEJ machinery between *S. pombe* and mammalian cells suggests that fission yeast may be a good model to investigate these processes, which probably represent new mechanisms of human inherited diseases.

I thank M. Ueno, P. Nurse, and Y. Hiraoka for generous gifts of strains and plasmid. I am grateful to T. Boon. I also thank M. Dutreix for helpful discussion and F. Foury, F. d'Adda di Fagagna, D. Hermand, B. Llorente, S. Marcand, and A. Goffeau for extremely useful comments on the manuscript. A.D. is supported by the Fonds National de la Recherche Scientifique.

LITERATURE CITED

Allen, C., C. A. Miller and J. A. Nickoloff, 2003 The mutagenic potential of a single double-strand break in a mammalian chromosome is not influenced by transcription. DNA Repair **2:** 1147–1156.

Anderson, D. E., K. M. Trujillo, P. Sung and H. P. Erickson, 2001 Structure of the Rad50·Mre11 DNA repair complex from *Saccharomyces cerevisiae* by electron microscopy. J. Biol. Chem. **276:** 37027–37033.

Baumann, P., and T. R. Cech, 2000 Protection of telomeres by the Ku protein in fission yeast. Mol. Biol. Cell **11:** 3265–3275.

Bentley, J., C. P. Diggle, P. Harnden, M. A. Knowles and A. E. Kiltie, 2004 DNA double strand break repair in human bladder cancer is error prone and involves microhomology-associated end-joining. Nucleic Acids Res. **32:** 5249–5259.

Boehm, T., L. Mengle-Gaw, U. R. Kees, N. Spurr, I. Lavenir *et al.*, 1989 Alternating purine-pyrimidine tracts may promote chromosomal translocations seen in a variety of human lymphoid tumours. EMBO J. **8:** 2621–2631.

Borensztajn, K., O. Chafa, M. Alhenc-Gelas, S. Salha, A. Reghis *et al.*, 2002 Characterization of two novel splice mutations in human factor VII gene causing severe plasma factor VII deficiency and bleeding diathesis. Br. J. Haematol. **117:** 168–171.

Boulton, S. J., and S. P. Jackson, 1996 *Saccharomyces cerevisiae* Ku70 potentiates illegitimate DNA double-strand break repair and serves as a barrier to error-prone DNA repair pathways. EMBO J. **15:** 5093–5103.

Boulton, S. J., and S. P. Jackson, 1998 Components of the Ku-dependent non-homologous end-joining pathway are involved in telomeric length maintenance and telomeric silencing. EMBO J. **17:** 1819–1828.

Campbell, C. L., and P. E. Thorsness, 1998 Escape of mitochondrial DNA to the nucleus in *yme1* yeast is mediated by vacuolar-dependent turnover of abnormal mitochondrial compartments. J. Cell Sci. **111:** 2455–2464.

Cao, L., E. Alani and N. Kleckner, 1990 A pathway for generation and processing of double-strand breaks during meiotic recombination in *S. cerevisiae*. Cell **61:** 1089–1101.

Chen, L., K. Trujillo, W. Ramos, P. Sung and A. E. Tomkinson, 2001 Promotion of Dnl4-catalyzed DNA end-joining by the Rad50/Mre11/Xrs2 and Hdf1/Hdf2 complexes. Mol. Cell **8:** 1105–1115.

D'Amours, D., and S. P. Jackson, 2002 The MRE11 complex: at the crossroads of DNA repair and checkpoint signalling. Nat. Rev. Mol. Cell Biol. **3:** 317–327.

Ding, D. Q., Y. Tomita, A. Yamamoto, Y. Chikashige, T. Haraguchi *et al.*, 2000 Large-scale screening of intracellular protein localization in living fission yeast cells by the use of a GFP-fusion genomic DNA library. Genes Cells **5:** 169–190.

Feldmann, E. X., V. X. Schmiemann, W. X. Goedecke, S. Reichenberger and P. Pfeiffer, 2000 DNA double-strand break repair in cell-free extracts from Ku80-deficient cells: implications for Ku serving as an alignment factor in non-homologous DNA end joining. Nucleic Acids Res. **28:** 2585–2596.

Goldin, E., S. Stahl, A. M. Cooney, C. R. Kaneski, S. Gupta *et al.*, 2004 Transfer of a mitochondrial DNA fragment to MCOLN1 causes an inherited case of mucolipidosis IV. Hum. Mutat. **24:** 460–465.

Gorbunova, V., and A. A. Levy, 1997 Non-homologous DNA end joining in plant cells is associated with deletions and filler DNA insertions. Nucleic Acids Res. **25:** 4650–4657.

Grimm, C., and J. Kohli, 1988 Observations on integrative transformation in *Schizosaccharomyces pombe*. Mol. Gen. Genet. **215:** 87–93.

Gu, Y., S. Jin, Y. Gao, D. T. Weaver and F. W. Alt, 1997 Ku70-deficient embryonic stem cells have increased ionizing radiosensitivity, defective DNA end-binding activity, and inability to support V(D)J recombination. Proc. Natl. Acad. Sci. USA **94:** 8076–8081.

Guirouilh-Barbat, J., S. Huck, P. Bertrand, L. Pirzio, C. Desmaze *et al.*, 2004 Impact of the Ku80 pathway on NHEJ-induced genome rearrangements in mammalian cells. Mol. Cell **14:** 611–623.

Heacock, M., E. Spangler, K. Riha, J. Puizina and D. E. Shippen, 2004 Molecular analysis of telomere fusions in *Arabidospis*: multiple pathways for chromosome end-joining. EMBO J. **23:** 2304–2313.

Heidenreich, E., R. Novotny, B. Kneidinger, V. Holzmann and U. Wintersberger, 2003 Non-homologous end-joining as an important mutagenic process in cell cycle-arrested cells. EMBO J. **22:** 2274–2283.

Huang, D., R. Giscombe, Y. Zhou, R. Pirskanen and A. K. Lefvert, 2000 Dinucleotide repeat expansion in the CTLA-4 gene leads to T cell hyper-activity via the CD28 pathway in myasthenia gravis. J. Neuroimmunol. **105:** 69–77.

Karathanasis, E., and T. E. Wilson, 2002 Enhancement of *Saccharomyces cerevisiae* end-joining efficiency by cell growth stage but not by impairment of recombination. Genetics **161:** 1015–1027.

Koike, M., 2002 Dimerization, translocation and localization of Ku70 and Ku80 proteins. J. Radiat. Res. **43:** 223–236.

Kramer, K. M., J. A. Brock, K. Bloom, J. K. Moor and J. E. Haber, 1994 Two different types of double-strand breaks in *Saccharomyces cerevisiae* are repaired by similar RAD52-independent, nonhomologous recombination events. Mol. Cell. Biol. **14:** 1293–1301.

Lander, E. S., L. M. Linton, B. Birren, C. Nusbaum, M. C. Zody *et al.*, 2001 Initial sequencing and analysis of the human genome. Nature **409:** 860–921.

Liang, F., M. Han, P. J. Romanienko and M. Jasin, 1998 Homology-directed repair is a major double-strand break repair pathway in mammalian cells. Proc. Natl. Acad. Sci. USA **95:** 5172–5177.

Lin, Y., and A. S. Waldman, 2001a Capture of DNA sequences at double-strand breaks in mammalian chromosomes. Genetics **158:** 1665–1674.

Lin, Y., and A. S. Waldman, 2001b Promiscuous patching of broken chromosomes in mammalian cells with extrachromosomal DNA. Nucleic Acids Res. **29:** 3975–3981.

Little, K. C. E., and P. Chartrand, 2004 Genomic DNA is captured and amplified during double-strand break (DSB) repair in human cells. Oncogene **23:** 4166–4172.

Longo, V. D., L. L. Liou, J. S. Valentine and E. B. Gralla, 1999 Mitochondrial superoxide decreases yeast survival in stationary phase. Arch. Biochem. Biophys. **365:** 131–142.

Ma, J.-L., E. M. Kim, J. E. Haber and S. E. Lee, 2003 Yeast Mre11 and Rad1 proteins define a Ku-independent mechanism to repair double-strand breaks lacking overlapping end sequences. Mol. Cell. Biol. **23:** 8820–8828.

Manivasakam, P., S. C. Weber, J. McElver and R. H. Schiestl, 1995 Micro-homology mediated PCR targeting in *Saccharomyces cerevisiae*. Nucleic Acids Res. **23:** 2799–2800.

Manolis, K. G., E. R. Nimmo, E. Hartsuiker, A. M. Carr, P. A. Jeggo *et al.*, 2001 Novel functional requirements for non-homologous DNA end joining in *Schizosaccharomyces pombe*. EMBO J. **20:** 210–221.

Mason, R. M., J. Thacker and M. P. Fairman, 1996 The joining of non-complementary DNA double-strand breaks by mammalian extracts. Nucleic Acids Res. **24:** 4946–4953.

Maundrell, K., 1993 Thiamine-repressible expression vectors pREP and pRIP for fission yeast. Gene **123:** 127–130.

Michel, B., S. D. Erlich and M. Uzest, 1997 DNA double-strand breaks caused by replication arrest. EMBO J. **16:** 430–438.

Moore, J. K., and J. E. Haber, 1996 Cell cycle and genetic requirements of two pathways of nonhomologous end-joining repair of double-strand breaks in *Saccharomyces cerevisiae*. Mol. Cell. Biol. **16:** 2164–2173.

Moreno, S., A. Klar and P. Nurse, 1991 Molecular genetic analysis of fission yeast *Schizosaccharomyces pombe*. Methods Enzymol. **194:** 795–823.

Mourier, T., A. J. Hansen, E. Willerslev and P. Arctander, 2001 The human genome project reveals a continuous transfer of large mitochondrial fragments to the nucleus. Mol. Biol. Evol. **18:** 1833–1837.

Okazaki, K., N. Okazaki, K. Kume, S. Jinno, K. Tanaka *et al.*, 1990 High-frequency transformation method and library transducing vectors for cloning mammalian cDNAs by trans-complementation of *Schizosaccharomyces pombe*. Nucleic Acids Res. **18:** 6485–6489.

Pâques, F., and J. E. Haber, 1999 Multiple pathways of recombination induced by double-strand breaks in *Saccharomyces cerevisiae*. Microbiol. Mol. Biol. Rev. **63:** 349–404.

Ricchetti, M., C. Fairhead and B. Dujon, 1999 Mitochondrial DNA repairs double-strand breaks in yeast chromosomes. Nature **402:** 96–100.

Ricchetti, M., F. Tekaia and B. Dujon, 2004 Continued colonization of the human genome by mitochondrial DNA. PLoS Biol. **2**(9): e273.

Richard, G.-F., B. Dujon and J. E. Haber, 1999 Double-strand break repair can lead to high frequencies of deletions within short CAG/CTG trinucleotide repeats. Mol. Gen. Genet. **261:** 871–882.

Richards, R. I., and G. R. Sutherland, 1997 Dynamic mutation: possible mechanisms and significance in human disease. Trends Biochem. Sci. **22:** 432–436.

Richly, E., and D. Leister, 2004 NUPTs in sequenced eukaryotes and their genomic organization in relation to NUMTs. Mol. Biol. Evol. **21:** 1972–1980.

Roth, D. B., P. B. Nakajima, J. P. Menetski, M. J. Bosma and M. Gellert, 1992 V(D)J recombination in mouse thymocytes: double-strand breaks near T cell receptor delta rearrangement signals. Cell **69:** 41–53.

Salomon, S., and H. Puchta, 1998 Capture of genomic and T-DNA sequences during double-strand break repair in somatic plant cells. EMBO J. **17:** 6086–6095.

Sargent, R. G., M. A. Brenneman and J. H. Wilson, 1997 Repair of site-specific double-strand breaks in a mammalian chromosome by homologous and illegitimate recombination. Mol. Cell. Biol. **17:** 267–277.

Schiestl, R. H., M. Dominska and T. D. Petes, 1993 Transformation of *Saccharomyces cerevisiae* with nonhomologous DNA: illegitimate

integration of transforming DNA into yeast chromosomes and in vivo ligation of transforming DNA to mitochondrial DNA sequences. Mol. Cell. Biol. **13:** 2697–2705.

Schiestl, R. H., J. Zhu and T. D. Petes, 1994 Effect of mutations in genes affecting homologous recombination on restriction enzyme mediated and illegitimate recombination in *Saccharomyces cerevisiae*. Mol. Cell. Biol. **14:** 4493–4500.

Seno, J. D., and J. R. Dynlacht, 2004 Intracellular redistribution and modification of proteins of the Mre11/Rad50/Nbs1 DNA repair complex following irradiation and heat-shock. J. Cell. Physiol. **199:** 157–170.

Shay, J. H., and H. Werbin, 1992 New evidence for the insertion of mitochondrial DNA into the human genome: significance for cancer and aging. Mutat. Res. **275:** 227–235.

Sun, H., D. Treco, N. P. Schultes and J. W. Szostak, 1989 Double-strand breaks at an initiation site for meiotic gene conversion. Nature **338:** 87–90.

Takeshige, K., M. Baba, S. Tsuboi, T. Noda and Y. Ohsumi, 1992 Autophagy in yeast demonstrated with proteinase-deficient mutants and conditions for its induction. J. Cell Biol. **119:** 301–311.

Teng, S. C., B. Kim and A. Gabriel, 1996 Retrotransposon reverse-transcriptase-mediated repair of chromosomal breaks. Nature **383:** 641–644.

Tomita, K., A. Matsuura, T. Caspari, A. M. Carr, Y. Akamatsu *et al.*, 2003 Competition between the Rad50 complex and the Ku heterodimer reveals a role for Exo1 in processing double-strand breaks but not telomeres. Mol. Cell. Biol. **23:** 5186–5197.

Tóth, G., Z. Gáspári and J. Jurka, 2000 Microsatellites in different eukaryotic genomes: survey and analysis. Genome Res. **10:** 967–981.

Tourmen, Y., O. Baris, P. Dessen, C. Jacques, Y. Malthiery *et al.*, 2002 Structure and chromosomal distribution of human mitochondrial pseudogenes. Genomics **80:** 71–77.

Turner, C., C. Killoran, N. S. T. Thomas, M. Rosenberg, N. A. Chuzhanova *et al.*, 2003 Human genetic disease caused by *de novo* mitochondrial-nuclear DNA transfer. Hum. Genet. **112:** 303–309.

Visser, W., E. A. van Spronsen, N. Nanninga, J. T. Pronk, J. Gijs Kuenen *et al.*, 1995 Effects of growth conditions on mitochondrial morphology in *Saccharomyces cerevisiae*. Antonie Van Leeuwenhoek **67:** 243–253.

Willett-Brozick, J. E., S. A. Savul, L. E. Richey and B. E. Baysal, 2001 Germ line insertion of mtDNA at the breakpoint junction of a reciprocal constitutional translocation. Hum. Genet. **109:** 216–223.

Wilson, S., N. Warr, D. L. Taylor and F. Z. Watts, 1999 The role of *Schizosaccharomyces pombe* Rad32, the Mre11 homologue, and other DNA damage response proteins in non-homologous end joining and telomere length maintenance. Nucleic Acids Res. **27:** 2655–2661.

Woischnik, M., and C. T. Moraes, 2002 Pattern of organization of human mitochondrial pseudogenes in the nuclear genome. Genome Res. **12:** 885–893.

Yu, X., and A. Gabriel, 1999 Patching broken chromosomes with extranuclear cellular DNA. Mol. Cell **4:** 873–881.

Yu, X., and A. Gabriel, 2003 Ku-dependent and Ku-independent end-joining pathways lead to chromosomal rearrangements during double-strand break repair in *Saccharomyces cerevisiae*. Genetics **163:** 843–856.

Zhong, Q., C.-F. Chen, P.-L. Chen and W.-H. Lee, 2002 BRCA1 facilitates microhomology-mediated end joining of DNA double strand breaks. J. Biol. Chem. **277:** 28641–28647.

Zhu, W. G., J. D. Seno, B. D. Beck and J. R. Dynlacht, 2001 Translocation of MRE11 from the nucleus to the cytoplasm as a mechanism of radiosensitization by heat. Radiat. Res. **156:** 95–102.

Communicating editor: A. Nicolas